ACS NANO

www.acsnano.org

ARTICLE

A Fiber Optic Interface Coupled to Nanosensors: Applications to Protein Aggregation and Organic Molecule Quantification

Daichi Kozawa,[§] Soo-Yeon Cho,[§] Xun Gong, Freddy T. Nguyen, Xiaojia Jin, Michael A. Lee, Heejin Lee, Alicia Zeng, Gang Xue, Jeff Schacherl, Scott Gibson, Leonela Vega, and Michael S. Strano*

Cite This: *ACS Nano* 2020, 14, 10141−10152

Read Online

ABSTRACT: Fluorescent nanosensors hold promise to address analytical challenges in the biopharmaceutical industry. The monitoring of therapeutic protein critical quality attributes such as aggregation is a long-standing challenge requiring low detection limits and multiplexing of different product parameters. However, general approaches for interfacing nanosensors to the biopharmaceutical process remain minimally explored to date. Herein, we design and fabricate a integrated fiber optic nanosensor element, measuring sensitivity, response time, and stability for applications to the rapid process monitoring. The fiber optic−nanosensor interface, or optode, consists of label-free nIR fluorescent single-walled carbon nanotube transducers embedded within a protective yet porous hydrogel attached to the end of the fiber waveguide. The optode platform is shown to be capable of differentiating the aggregation status of human immunoglobulin G, reporting the relative fraction of monomers and dimer aggregates with sizes 5.6 and 9.6 nm, respectively, in under 5 min of analysis time. We introduce a lab-on-fiber design with potential for at-line monitoring with integration of 3D-printed miniaturized sensor tips having high mechanical flexibility. A parallel measurement of fluctuations in laser excitation allows for intensity normalization and significantly lower noise level (3.7 times improved) when using lower quality lasers, improving the cost effectiveness of the platform. As an application, we demonstrate the capability of the fully integrated lab-on-fiber system to rapidly monitor various bioanalytes including serotonin, norepinephrine, adrenaline, and hydrogen peroxide, in addition to proteins and their aggregation states. These results in total constitute an effective form factor for nanosensor-based transducers for applications in industrial process monitoring.

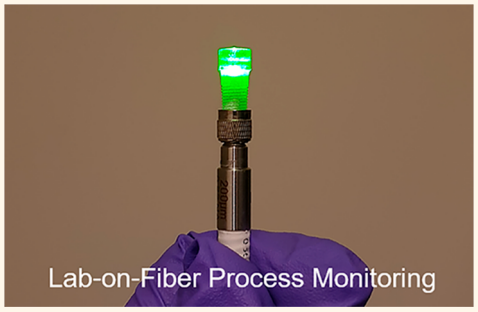

KEYWORDS: *optode fiber, biopharmaceutical monitoring, protein aggregation, carbon nanotube, lab on fiber, antibody*

Pharmaceutical manufacturing involves a series of complex processing steps including extraction, purification, and polishing.[1] Protein and macromolecular therapeutics in particular need to be controlled for stability with respect to aggregation caused by aberrant processing and storage conditions such as excessive heat, light, shear, ionic strength, and pH.[2,3] Undesired aggregates include monomer−monomer nucleation and aggregate−aggregate coalescence, resulting in particles ranging from 10 nm to greater than 10 μm.[4] Protein products that remain correctly folded upon aggregation still possess limited solubility limiting the maximum dosage of drug. Also, changes in solution viscosity inhibit intramuscular or subcutaneous delivery.[5−7] Protein aggregation can also induce immunogenic responses, the onset of autoimmune disease.[8,9] There is an increased need from both a safety and regulatory standpoint for rapid diagnostics that can monitor product quality, specifically to discern monomers from dimers, trimers, and polymers.[10] As a potential solution, nanotechnology-enabled sensors, such as those based on carbon nanotubes,[11] graphene,[12] or plasmonic nanoparticles,[13] exhibit ultralow detection limits and rapid transduction time due to high surface areas.[14] However, the conceptual design and fabrication of an interface between such

Received: April 23, 2020
Accepted: July 15, 2020
Published: July 15, 2020

https://dx.doi.org/10.1021/acsnano.0c03417
ACS Nano 2020, 14, 10141−10152

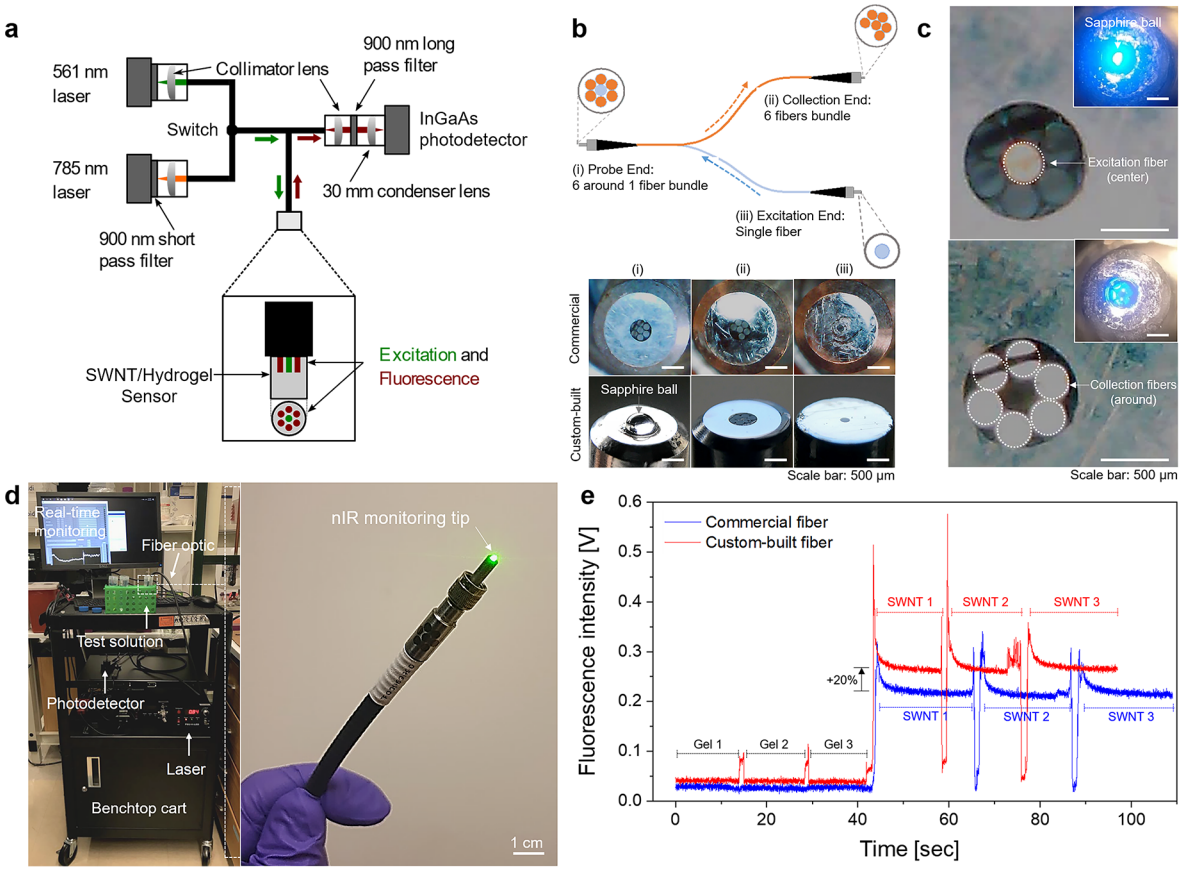

Figure 1. Fabrication and testing of fiber optic instrumentation for nanosensor interfacing. (a) Schematics of optode fiber configuration with excitation sources, photodetector, and the nanosensor system. (b) Schematics and photo images of the optode fiber configurations with commercial (top) and custom-built probes (bottom). (c) Optical microscope images of probe fiber tips with excitation and fluorescence collection components (inset: sapphire half ball lens included with custom-built variants). (d) Photo image of the fully integrated fiber optic benchtop instrument with benchtop mobile cart. (e) Fluorescence collection performance comparison between commercial and custom-built optode fibers.

sensors and a form factor compatible with online or at-line monitoring of a pharmaceutical manufacturing process is lacking in the literature. In this work, we address this gap by designing and implementing a fiber optic interface that serves this purpose.

A wide variety of analytical methods are utilized to quantify organic molecules, even during chemical manufacturing.[15] However, proteins in particular must be monitored for aggregation as described above. To this end, conventional methods including high-performance liquid chromatography (HPLC),[16] dynamic light scattering (DLS),[17] capillary electrophoresis,[18] and single-particle tracking (SPT)[19,20] have been widely used with different levels of complexity and assay time. Despite considerable progress, critical limitations remain in both speed and quantification resolution: these techniques vary in the amount and resolution of structural and size information that they provide, with no single analytical technique being capable of fully elucidating the quantitative protein size distribution.[20−22] Additionally, these analytical tools remain challenging to implement as online or at-line monitoring devices.[23] Thus, there is a need for the development of new analytical technologies capable of measuring target proteins rapidly with resolution at the monomer level. More importantly, the analytical technology should be portable and easily coupled to existing benchtop instruments for quality assessment as part of the online or at-line production process.[23,24]

Nanosensors including single-walled carbon nanotubes (SWNTs) are promising approaches toward rapid, label-free, and single molecule level biopharmaceutical characterization and have been developed for glycoprotein characterization,[25] biomarker detection,[26] and characterization of protein-binding interactions.[27] Their optical readout is well suited for sensor multiplexing, in which nanosensor arrays were fabricated and characterized for protein detection.[28] However, despite these advantages it is not clear how to formulate such sensors into an interface to the process environment.

In this work, we develop a fiber optic (optode) benchtop platform that interfaces the advantages of nanoparticle-based sensors with a probe form factor compatible with industrial process monitoring. We demonstrate the utility with the dynamic monitoring of protein aggregation, a challenging problem in pharmaceutical manufacturing. The optode consists of a single optical fiber that performs both the excitation and signal collection component of fluorescent nanosensor evaluations. The sensor element consists of chitosan-wrapped SWNT nanosensors with excitation and emission in the visible and near-infrared (nIR) ranges, respectively. With the optode fiber's small form factor and mechanical flexibility, all the components including optode fiber, laser, nanosensors, nIR detectors, and measurement

https://dx.doi.org/10.1021/acsnano.0c03417
ACS Nano 2020, 14, 10141−10152

instrument are compactly and fully integrated into a single portable benchtop platform, which can be easily and directly applied to pharmaceutical processing steps with at-line analysis. Using this setup, we demonstrate the differentiation of immunoglobulin G (IgG) from 5.6 nm monomers to 9.6 nm dimer aggregates as well as bioanalytes including serotonin, norepinephrine, adrenaline, and hydrogen peroxide. Finally, the lab-on-fiber monitoring system is demonstrated with integration of user-defined 3D-printed miniaturized sensing tips.

RESULTS AND DISCUSSION

Our overall strategy for optode development is divided into two steps: (1) development of the optical fiber for excitation and collection of a nanosensor tip and (2) attachment of an optically coupled hydrogel with embedded nanosensors to the optical fiber end, facilitated by 3D-printed adaptors for this purpose.

For step (1), our design of the optode fiber and associated instrumentation are illustrated in the schematics of Figure 1a. The tool contains an optical fiber bundle coupled to dispersed nanosensors immobilized within a agarose hydrogel matrix. The hydrogel allows for direct immersion of the optode tip into complex liquid samples while maintaining the coupling to both excitation and the InGaAs-amplified photodetector as a collection. Fluorescent SWNT nanosensors were excited with both 561 and 785 nm lasers with the ability of the system to be automatically switched depending on the chirality of the SWNT in the hydrogel (optical ray tracing simulations of coupling multiple light sources are shown in Figure S1). For example, 561 nm light is resonant with the band gap (the second gap E_{22}) of (6, 5) chirality, while 785 nm light is resonant with high-pressure carbon monoxide (HiPCO) SWNT including (10, 2), (9, 4), (8, 6), and (8, 7) chiralities. In this work, 561 nm lasers were chosen for the fluorescence measurements. The schematic (top) and micrographs (bottom) of Figure 1b show the detailed configurations of the optode fibers for biochemical monitoring. The fiber optic probe is composed of a simple six-around-one fiber bundle where the central fiber provides the laser excitation for the SWNT nanosensors in the hydrogel. The surrounding six fibers then collect the nIR fluorescence signal from the nanosensor element. Two different kinds of optode fibers were tested and used as part of this project. The first fiber is commercially available from Thorlabs, Inc., made up of bundles of multimode fibers, but does not contain any end micro-optics (images, top). The second fiber is a custom-built fiber optic probe with end micro-optics fabricated in our group as described in Figures S2−S7. The latter fiber was also made with six multimode optical fibers around a center multimode optical fiber (images, bottom). A sapphire half ball lens is added at the tip of the fiber bundles to improve the angle at which the fluorescence light from the center fiber illuminates the sensor element while at the same time increasing the collection angle of the anisotropic near-infrared fluorescence from the SWNT nanosensors. This custom-built fiber was specifically designed and fabricated to confirm whether the modified probe with end micro-optics end could improve nIR detection or not. Optical microscope images of the sensing tips of both commercial and custom-built fibers (insets, top-right) show that excitation and collection fibers were properly integrated with the appropriate light paths (Figure 1c).

Figure 1d shows images of the fully integrated benchtop instrument for process monitoring. All components including the optode fiber, laser, nanosensors, nIR detectors, monitor, controller, and test solutions are compactly integrated onto a benchtop mobile cart (depth 18 in., width 24 in., height 26−42 in.). In addition, the magnified image (right) shows that the optode fiber is flexible, lightweight, and robust enough such that the tip could be easily applied to reaction batches or process monitoring sites that would be difficult with conventional analytical tools. Finally, the fluorescence intensities of the commercial and custom-built optode fibers were compared (Figure 1e). The nIR monitoring tip of each optode fiber was moved well to well of a 96-well plate with gel 1 to gel 3 for reference (without SWNT) and then moved to SWCNT 1 to SWCNT 3, where the difference between the intensities of the SWCNT and gel corresponds to fluorescence intensity from the SWCNT. It is clearly observed that reference gel wells without SWNT do not show any fluorescence signal, while bright signal is observed with SWNT-containing gel wells. Especially, the custom-built optode fiber improves the fluorescence intensity of the SWNT within a 20% scale (from 0.21 to 0.25 V) due to effective fluorescence capture from the sapphire half ball lens on the tip. Thus, the optode fiber tip with micro-optics can definitely improve collection efficiency. However, since multiple fabrication steps are needed for the custom-built fiber version with micro-optics and the commercial probe is readily available at minimal cost (typically $418.14 at Thorlabs, Inc.), the commercial optode fiber is employed for the rest of this study.

To be cost-effective and flexible as an optode fiber system, it may be more practical to employ lower quality lasers for excitation, due to their considerably lower price. But the resulting power fluctuations in time can compromise detection limits, as shown in the noisy signals of Figure 1e. Improvements in nanosensor performance cannot compensate for this, and the higher noise prevents at-line monitoring in an industrial setting. To address this, we have developed a parallel-measurement system that samples the real-time delivered power in parallel to the optode fiber response. Nanosensor fluorescence intensity is ideally proportional to laser power, and fluctuations in excitation necessarily lead to increase noise levels.[29] It is possible to cancel out the laser fluctuations by integrating a power meter as shown in the inset of Figure S8. The signal can then be normalized as follows:

$$I(t) = \frac{I_{\text{fluorescence}}(t)}{I_{\text{power meter}}(t)/I_{\text{power meter}}(0)} \quad (1)$$

where the fluorescence intensity is $I_{\text{fluorescence}}(t)$ and the measured power on the power meter is $I_{\text{power meter}}(t)$. Note that the measured laser power is position dependent in this configuration. The baseline noise profile is significantly reduced from 4.47% to 1.2% level fluctuations (3.7 times improved) with the power meter monitoring systems. Accordingly, we also normalized the measured power as read at the meter. It is clearly seen that baseline noise profile is significantly improved with this approach. Overall, the strategy described in step (1) above of fiber optic integration is successful.

Our fully integrated optode fiber instrument aims for an at-line form factor to detect biopharmaceutical aggregation and process impurities. As a proof of concept, a 96-well plate with SWNT sensors immobilized in a hydrogel was employed as an

https://dx.doi.org/10.1021/acsnano.0c03417
ACS Nano 2020, 14, 10141−10152

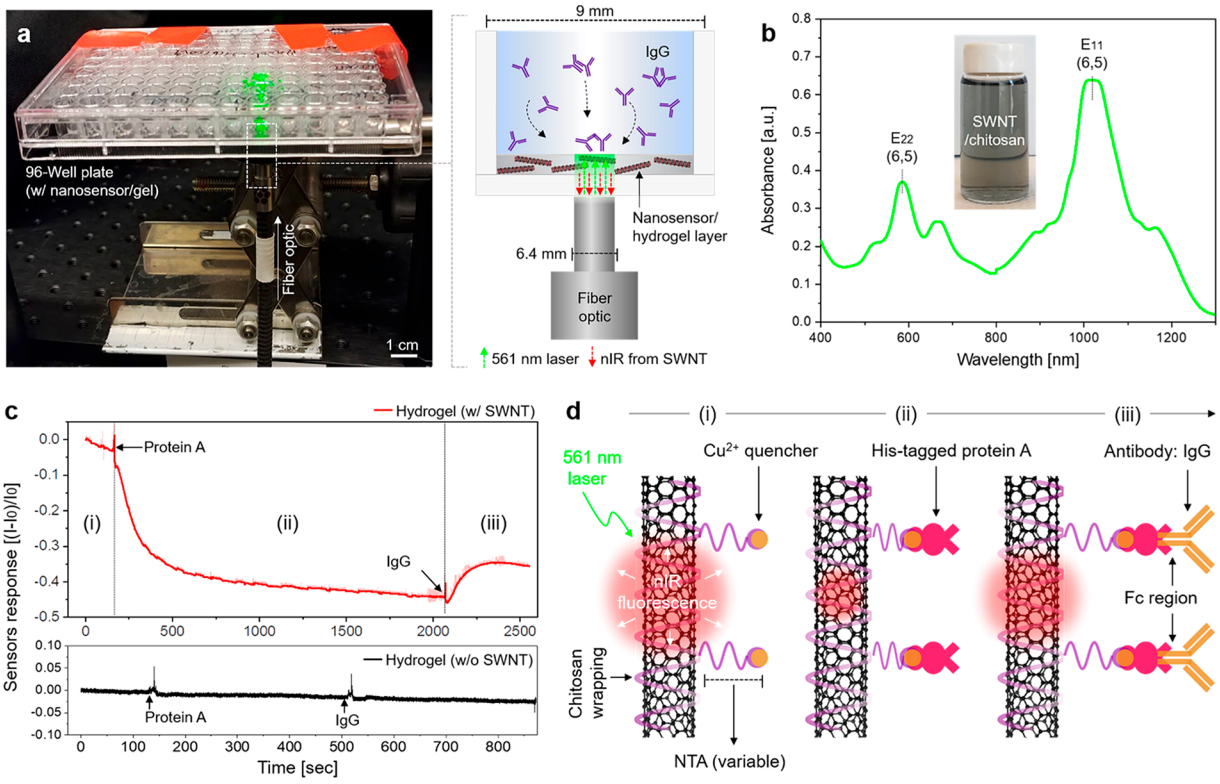

Figure 2. Testing of the optode fiber with an uncoupled system (96-well plate) collecting responses from the nanosensor/hydrogel confirming successful excitation and emission collection. (a) Photo image (left) and schematics (right) of measurement configurations with a 96-well plate, SWNT/hydrogel sensors, and optode fiber. (b) UV−vis−nIR absorbance spectrum of chitosan-wrapped SWNT nanosensors (inset: photo image of the nanosensor dispersion). (c) Hydrogel signal modulation with and without SWNT sensor encapsulation following protein A and unstressed human antibody IgG injections. (d) Schematic of the nanosensor detection mechanism of IgG with the turn-off and turn-on response of the His-tagged protein A system.

at-line measurement form factor for the uncoupled system since the plate allows users to prepare replicate samples producing measurements with consistent optics. Figure 2a shows the image and schematic of the measurement configuration with this 96-well plate, nanosensor/hydrogel, and optode fiber. The nIR monitoring tip of the optode fiber was attached on the bottom surface of a 96-well plate and collected the nIR signals from the nanosensor. The SWNT transducers were immobilized in a porous hydrogel matrix (0.2% agarose), which can efficiently modulate the selective diffusion of antibody proteins to the SWNT layer, allowing us, in this example, to identify the presence of aggregate species through changes in the sensor response dynamics. In contrast to a sensor built on a chip substrate, the integration of a transducer on an optical fiber allows for remote testing with distance from the target; thus, the monitoring tip of the optode fiber does not require precise focusing (Figure S9). Accordingly, the benchtop instrument allows for rapid prototyping with minimal training. Protein A-modified fluorescence SWNTs (purified (6, 5) chiralities provided by Chasm Advanced Materials (CHASM)) with chitosan functionalization were exploited as a transducer for IgG aggregation monitoring with an optode fiber. To preattach the protein A on the SWNT/chitosan nanosensors, Cu-N^{α},N^{α}-bis(carboxymethyl)-L-lysine hydrate (Cu-NTA) was covalently bonded with carboxylic acid groups of chitosan-functionalized SWNT surfaces (the detailed synthesis mechanism of the nanosensor is described in the Methods section). The UV−vis−nIR absorbance spectrum of the nanosensor dispersion clearly shows the significant E_{22} (6, 5) and E_{11} (6, 5) absorbance peaks at 584 and 1014 nm, respectively, indicating that SWNT surfaces were well functionalized with chitosan chemistry and dispersed in the solution phase (Figure 2b, inset: image of the nanosensor dispersion).[27]

The dynamic fluorescence response of the SWNT/chitosan nanosensors immobilized in a hydrogel was measured during a single injection of protein A and IgG in series (Figure 2c). The sensor response is defined as $R(t) = (I(t) - I_0)/I_0$, where I_0 is the initial fluorescence intensity and $I(t)$ is the fluorescence intensity at time t. Nanosensor response from the optode fiber showed a nIR quenching response with protein A injection and drastically recovered to the 65% level of the original fluorescence intensity following IgG (10 μL of 10 mg/mL) injection. The hydrogel without the SWNT nanosensor did not show any fluorescence response to protein A and IgG injection, indicating that the signal is not from any additional sources such as mechanical deformation of the gel or liquid flowing effect (bottom graph of Figure 2c). These dynamic responses are consistent with our previous measurement in a conventional nIR fluorescence instrument.[27,30] In addition, our optode fiber showed consistent IgG-detecting response even with various SWNT chiralities (CHASM (6, 5) and HiPCO (10, 2), (9, 4), (8, 6), and (8, 7)), indicating that our fiber optic platform can be applied to various fluorescence measurement with high reliabilities (Figure S10). Various concentrations of IgG samples were monitored with the optode fiber nanosensor, and the limit of detection was determined to be below 660 nM, which is almost identical with

https://dx.doi.org/10.1021/acsnano.0c03417
ACS Nano 2020, 14, 10141−10152

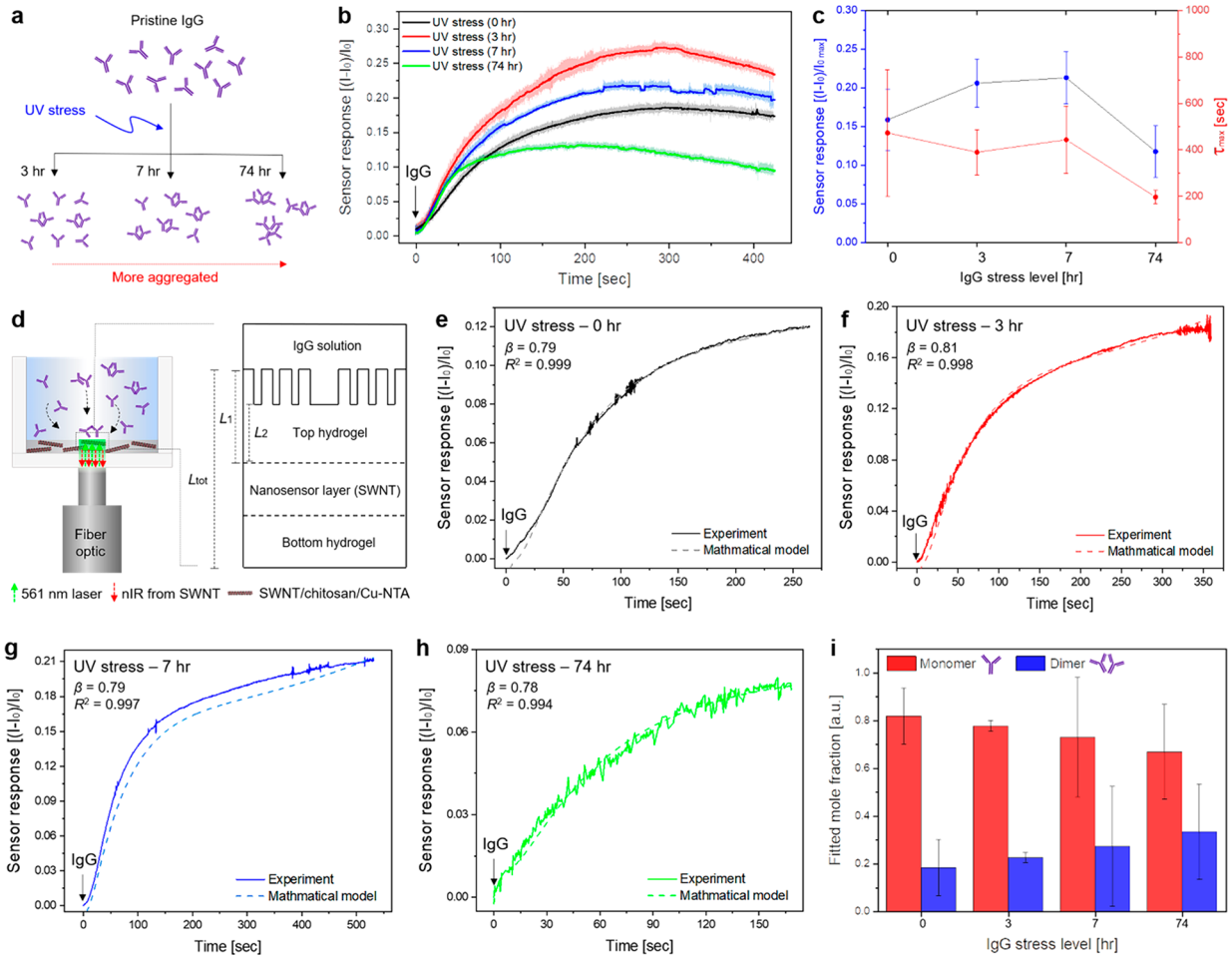

Figure 3. IgG aggregation monitoring performance of an optode fiber with an uncoupled system. (a) Schematics of IgG aggregation behavior with UV exposure of 3, 7, and 74 h. (b) Real-time fluorescence response of the nanosensor with an optode fiber to 0, 3, 7, and 74 h stressed IgG (10 μL of 10 mg/mL, after protein A priming). (c) Maximum sensor response ($((I(t) - I_0)/I_0)_{max}$) and the time at maximum response (t_{max}) to 0, 3, 7, and 74 h stressed IgG. (d) Schematics of the SWNT/hydrogel sensing system described by a multilayer diffusion model with two different hydrogel thicknesses, L_1 and L_2. Dynamic sensing responses to various stress times of IgG ((e) 0 h, (f) 3 h, (g) 7 h, and (h) 74 h) with the derived model fitting. (i) Statistics of model-extracted mole fractions of monomer (α_{MP}) and dimer (α_{HMW}) IgG. The error bars are standard deviations of experiments with triplicate sensor synthesis.

the conventional offline IgG monitoring performances (Figure S11).[27,30] Overall, these measurements show the capability of observing the fluorescence change of nanosensors using the optode fiber system with excitation and collection optics. The schematics in Figure 2d describe the detailed mechanisms of the nIR fluorescence quenching and turn-on responses of SWNT/chitosan nanosensors in a hydrogel.[15,30] At the initial state (i), Cu-NTA is covalently bonded with carboxylic acid groups of the chitosan surface of the SWNT as described earlier, and the Cu^{2+} ion of Cu-NTA works as a proximity quencher of SWNT fluorescence. We hypothesize that His-tagged protein A is bound to Cu-NTA and results in a change in intermolecular distance between the SWNT and the Cu^{2+}, leading to the quenching response of nIR signals (state (ii)). Finally, when test solutions are injected onto the nanosensor/hydrogel layers, IgG is bound to protein A with strong affinity to the fragment crystallizable (Fc) region of IgG. Then, the attached Cu^{2+} quencher is pulled away from the SWNT surface and fluorescence intensities are recovered, leading to a drastic nIR turn-on response (state (iii)). In accordance with this, IgG injection without protein A does not show any fluorescence responses of the optode fiber since IgG could not form Fc binding with protein A, which does not lead to quencher spacing variation (Figure S12). Consequently, it is clearly demonstrated that our optode fiber interfaced nanosensor could be used for real-time monitoring of protein A and IgG chemical reactions.

In order to investigate the IgG aggregation monitoring performance of the optode fiber system, nIR fluorescence of the partially aggregated IgG that underwent various stress levels of ultraviolet (UV) light irradiation for 0, 3, 7, and 74 h was measured using an uncoupled system (Figure 3). Previous works demonstrated that higher portions of IgG were aggregated with higher exposure time to UV light since light exposure leads to photo-oxidations (Figure 3a).[31,32] In order to investigate the reliability and analyze with statistics on sensor responses, the measurements were conducted three times on each stress level of IgG with the identical conditions. Dynamic fluorescence responses of the nanosensors measured by optode fiber showed that the sensors show quick turn-on responses ($(I - I_0)/I_0$ up to 0.275) to all levels of aggregated IgG within 4 min (Figure 3b). Especially, for the 74 h stressed IgG, the sensor showed immediate saturation behavior with a short response time (~100 s) and lower turn-on response amplitude

https://dx.doi.org/10.1021/acsnano.0c03417
ACS Nano 2020, 14, 10141−10152

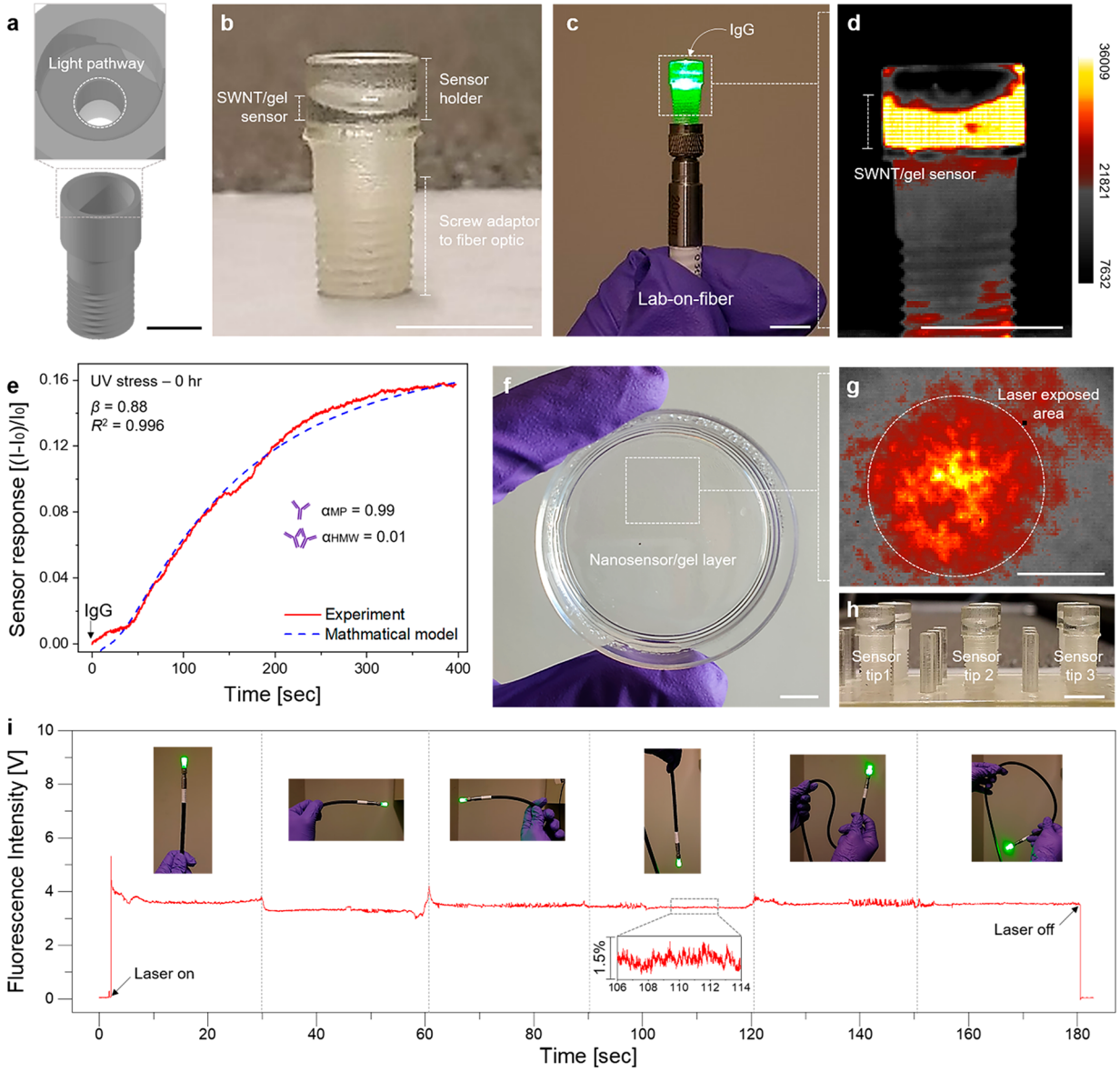

Figure 4. Fully integrated lab-on-fiber protein monitoring system coupled with a 3D-printed miniaturized sensor tip. (a) CAD of a sensor tip for 3D-printing. Photo image of (b) pristine 3D sensing tip with nanosensor/hydrogel and (c) fully integrated optode fiber system. (d) Magnified nIR image of the 3D-printed sensor tip with an excitation laser. (e) Real-time sensor response and model fitting of a 3D sensor tip coupled with an optode fiber to unstressed IgG (10 μL of 10 mg/mL). (f) Photo image of the SWNT/hydrogel sensing layer synthesized in large scale (5.5 cm Petri dish). (g) Magnified nIR image of the large-area synthesized SWNT/hydrogel sensing layer with maximum beam size exposure. (h) Multiple prefabricated sensing tip array for readily interfacing with an optode fiber. (i) Real-time fluorescence signal of a fully integrated lab-on-fiber system with varied mechanical distortions during measurement (scale bars: 1 cm).

$((I - I_0)/I_0 \approx 0.125)$. Figure 3c shows the maximum sensor response $((I(t) - I_0)/I_0)_{max}$) and the time at the maximum response t_{max} calculated from real-time response data. It is clearly seen that the maximum response amplitudes and t_{max} to 74 h stressed IgG are much smaller than those of 0, 3, and 7 h stressed IgG. This might be due to the highly stressed samples containing large-size IgG aggregates with a high concentration of oxidized species, which induces difficult binding of protein A and the Fc receptor.[33,34] On the contrary, 0, 3, and 7 h stressed IgG showed identical time-series reactions; however, the maximum responses and t_{max} of responses to 0, 3, and 7 h are insufficient to differentiate aggregation levels of each IgG sample. The slight increase from 0 h to 3 and 7 h stressed IgG could be attributed to slightly different concentrations of IgG stock solutions (±15%), which is already observed by an absorbance study of previous work.[30] Accordingly, it requires further precise mathematical modeling of the response curves for each stress level, as we discuss below.

We have adapted a multiphase hydrogel diffusion model to predict the response of the optode fiber with a nanosensor and precisely analyze the IgG aggregation status. The setup of the problem follows the mathematical diffusion model developed previously.[35,36] The development below allows us to quantitatively describe the turn-on response of SWNT nanosensors embedded in a multiphase hydrogel on the end of an optode fiber upon addition of IgG. The diffusion model consists of SWNT immobilized in an agarose hydrogel layer with two thickness: (i) thickness L_1 from the top surface of the hydrogel to the sensor layer and (ii) thickness L_2 from the lower top surface of the hydrogel to the sensor layer that

https://dx.doi.org/10.1021/acsnano.0c03417
ACS Nano 2020, 14, 10141−10152

accounts for cracks within the hydrogel layer formed during casting and/or heterogeneity in the hydrogel thickness (Figure 3d). Then, the total concentration profile in the two diffusion models with a time scale could be expressed as the following equation.

$$C_T(t) = \alpha_{MP}C_0\left[\beta\frac{C_{MP}(L_1, t)}{C_0} + (1-\beta)\frac{C_{MP}(L_2, t)}{C_0}\right] + \alpha_{HMW}C_0\left[\beta\frac{C_{HMW}(L_1, t)}{C_0} + (1-\beta)\frac{C_{HMW}(L_2, t)}{C_0}\right] \quad (3)$$

where α_{MP} is the mass fractions of the monomer, α_{HMW} is the high molecular weight (HMW) IgG to total IgG weight, L_1 is the smaller layer, and β is the ratio of the thick hydrogel layer (detailed model derivation in Supporting Information S7). Equation 3 is fitted to the dynamic responses of the nanosensor measured by the optode fiber to 0, 3, 7, and 74 h stressed IgG, and the fitting parameters were extracted (Figure 3e−h, respectively). The HMW species were assumed as dimers for the model, and the hydrodynamic radii were approximated as 5.6 and 9.6 nm for monomer and HMW species, respectively, with statistics on previously reported works.[30,37,38] First of all, it is clearly seen that all the measured data were well fitted with expected dynamics with eq 3, having a mean R^2 value of near 1 (0.9990, 0.9989, 0.9968, and 0.9944 for 0, 3, 7, and 74 h, respectively). The extracted β values of each experiment were 0.79, 0.81, 0.79, and 0.78 for 0, 3, 7, and 74 h stressed IgG, respectively, demonstrating that microwell cross-sectional compositions of all three samples were identical, and consequently only the aggregation status of each IgG affected the response dynamics. More importantly, it is clearly observed that the average α_{MP} decreases (0.82, 0.77, 0.72, 0.66) and α_{HMW} increases (0.18, 0.22, 0.27, 0.33) with the longer UV exposure time since IgG is aggregated into high molecular weight drastically as expected (Figure 3i). This monomer and aggregated dimer ratio extracted by our optode fiber system showed a similar tendency to the ratio confirmed by size-exclusion ultrahigh-performance liquid chromatography (SE-UPLC).[30] Overall, it is clearly demonstrated that our optode fiber benchtop instrument with nanosensor interfacing successfully differentiated the various aggregation levels of IgG with mathematical modeling. A previous diffusion model for offline IgG monitoring was identically applied on our system, indicating that our fiber optics could be used as a reliable form factor for interfacing a nanosensor into the field-oriented applications. In addition, it is a strength to be able to fit the diffusion model to the uncoupled system, showing that no additional fitting of parameters is needed for the real coupled system shown at the end.

Indeed, the microscopic cross-section and high aspect ratio combined with mechanical robustness and flexibility make our optode fiber an unrivaled candidate for lab-on-fiber technology.[39,40] The sensing tip of the optode fiber could be easily applied on various shapes/types of chemical reaction batches or fluorescent monitoring sites. Accordingly, it could efficiently be applied to a small form factor for at-line monitoring in the biopharmaceutical industry.[41] In order to demonstrate the lab-on-fiber with our optode fiber benchtop instrument, a three-dimensional (3D) miniaturized sensor tip was designed and fabricated by 3D-printing. Figure 4a shows the computer-aided design (CAD) of a miniaturized sensor tip for 3D-printing. The design has a 7 mm scale miniaturized circular chamber for holding the nanosensor/hydrogel layer and screw-shaped pillar, which allows the mold to be integrated with the end of the optode fiber. In addition, a 3.5 mm size hole is in the center of the sensor tip, which allows excitation light to directly touch the nanosensor/hydrogel and collect the fluorescence signal sensitively. Accordingly, the probe end of the fiber does not physically contact the SWNT/hydrogel layers, indicating that the surface of the probe ends could be protected from any chemical contamination and fouling problems. The sensor tips were printed by a 3D-printer (Objet 30 Prime, Stratasys Ltd.) using methacrylate photopolymers and cured in UV light at a 60 °C controlled temperature. After 3D-printing, the printed molds were washed in isopropyl alcohol (IPA) to remove residual resin overnight. Figure 4b shows the photo image of the printed 3D sensing tip integrated with the SWNT/hydrogel sensors. It is clearly seen that the millimeter-scale solid 3D polymer mold is well printed with a precise screw adaptor and holds the SWNT/hydrogel sensing layer stable. Since our sensing tip for the optode fiber was exquisitely designed with high-resolution (millimeter-scale) 3D architecture, protein aggregation status could be sensitively monitored even with very small amounts of target batch solutions (<10 μL). More importantly, the printed 3D sensing tip was successfully integrated with the optode fiber by screwing into an SMA (subminiature version A) connector for a lab-on-fiber protein monitoring system (Figure 4c). A magnified nIR image with an excitation laser showed that intensive fluorescence signals were emitted from selective regions of the sensor holder, demonstrating that the nanosensors were well integrated in a predefined location of the 3D sensing tip (Figure 4d). Figure 4e shows the real-time fluorescence response of the fully integrated optode fiber to unstressed IgG. A 10 μL amount of analyte solution was directly dropped on the 3D sensing tip of the optode fiber, and the sensor response was directly measured with our benchtop instrument. It is noticeable that the measured response from the 3D sensing tip showed identical turn-on behavior and similar response amplitude to the sensing signal from the nanosensor of the uncoupled system (96-well plate). Furthermore, the response from the fully integrated optode fiber is well fitted (R^2 = 0.9963) by our multiphase hydrogel diffusion model above with a fitting parameter of β = 0.88, respectively, indicating that the hydrodynamics of the nanosensor layer in the 3D sensing tip was identical with the uncoupled system. More importantly, extracted α_{MP} and α_{HMW} were 0.99 and 0.01, respectively, demonstrating that the nonaggregated protein status of 0 h stressed IgG was perfectly monitored by the fully integrated optode fiber system. Consequently, it is clearly shown that our optode fiber could be efficiently applied to lab-on-fiber technology with a 3D sensor tip for protein aggregation monitoring.

Our design for the 3D sensor tip allows potential users to easily exchange the used SWNT/hydrogel sensors in the holder to render the sensor element a disposable component. To demonstrate this, the SWNT/hydrogel sensing layer is synthesized in large area (centimeter scale) and integrated with a multiple 3D sensor tip array. The photo image shows that a thin and uniform layer of the SWNT/hydrogel sensor is synthesized on a 5.5 cm scale circular Petri dish without any defects or aggregation (Figure 4f). In addition, strong nIR signals were clearly measured from the whole exposed area of the SWNT/hydrogel layer with an excitation laser, indicating that multiple sensing tips having reliable fluorescent properties

https://dx.doi.org/10.1021/acsnano.0c03417
ACS Nano 2020, 14, 10141−10152

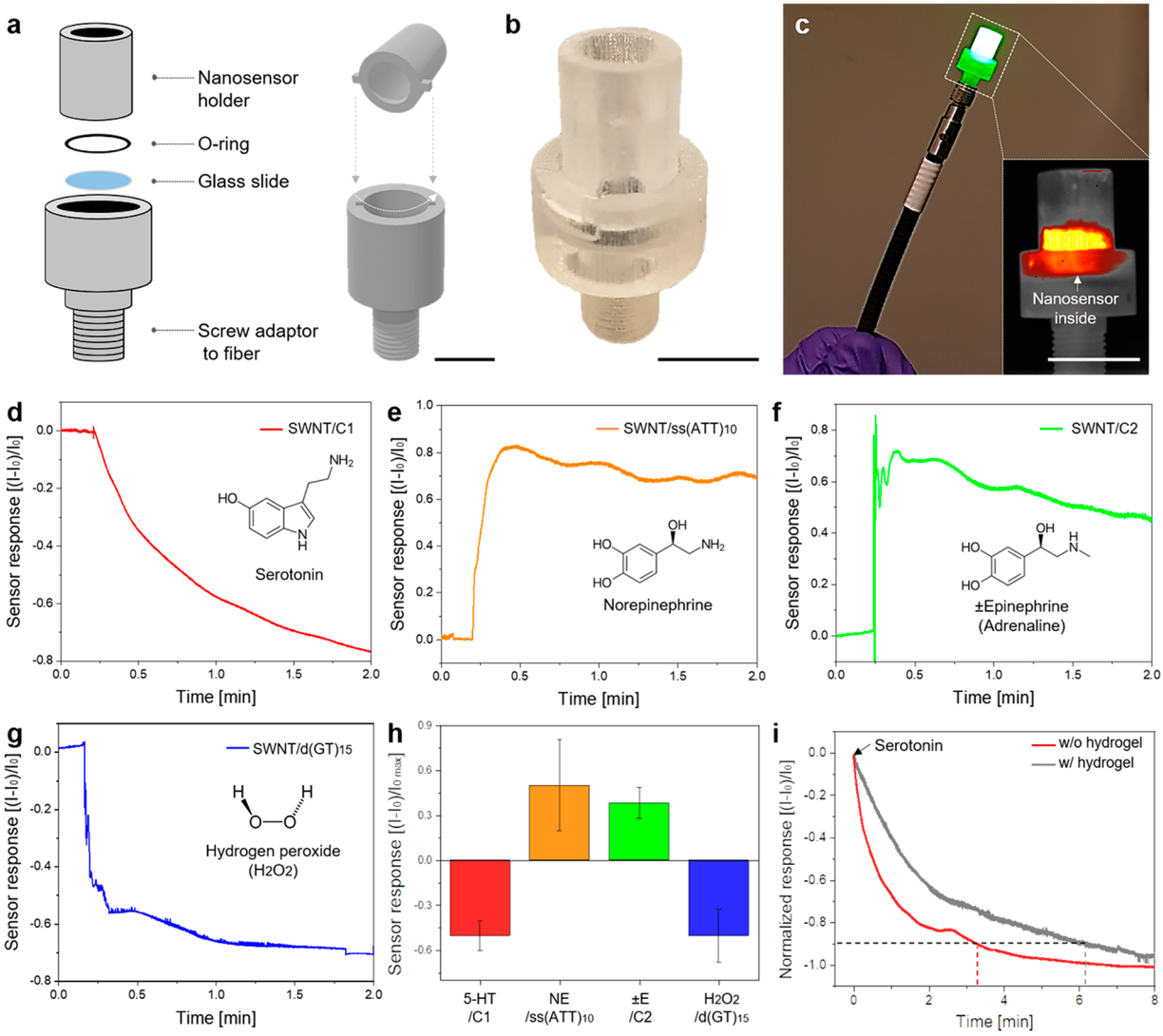

Figure 5. Extension of the optode fiber to other bioanalytes of interest, employing an alternate 3D sensor tip design. (a) Schematics and CAD for the 3D miniaturized sensor tip configuration for liquid phase nanosensor detection, without the hydrogel interface. (b) Image of the assembled nanosensor tip with an O-ring and glass slide. (c) Fully integrated sensor tip for liquid phase bioanalyte detection (inset: nIR image of 3D sensor tip with excitation laser). Real-time lab-on-fiber monitoring of various bioanalytes (5 μL) including (d) serotonin (5-HT) (1 mM), (e) norepinephrine (NE) (1 mM), (f) ±epinephrine (adrenaline) (1 mM), and (g) hydrogen peroxide (H_2O_2) (10 mM). (h) Maximum sensor response following a 2 min exposure with each analyte. (i) Normalized sensor response of 3D sensing tip with and without hydrogel for 1 mM serotonin (scale bars: 1 cm).

could be easily prepared by mass production of nanosensor/hydrogel components (Figure 4g). Considering the size of the miniaturized sensor tip, theoretically a maximum of 61 sensor tips could be prepared with just a single synthesis of the SWNT/hydrogel on a 5.5 cm scale Petri dish. In addition, a multiple sensing tip array was fabricated with a single printing of a 3D-printer and could hold the multiple SWNT/hydrogel sensors from presynthesized large-area layers, which allows them to be readily interfaced with the optode fiber (Figure 4h). Accordingly, users can easily conduct protein/drug status measurements just by changing the sensor tip of an optode fiber with a previously fabricated new tip, which is a real application for online and at-line lab-on-fiber technology. In order to investigate the maximum measurement counts of a single sensor tip, the SWNT/hydrogel sensor response to three repetitive IgG injections was measured (Figure S13). It is observed that the optode fiber response became slightly smaller for the second injection of IgG and finally saturated with the third injection of IgG. This might be due to the fact that an excess amount of IgG may get stacked at the nanopores of the hydrogel. Thus, our disposable single sensor tip can be used twice for measurements and then be replaced with a new sensor tip.

Finally, to investigate the mechanical robustness and flexibility of our fully integrated lab-on-fiber system, the real-time nIR baseline was continuously measured during simultaneous fiber deformation into various shapes (Figure 4i). After laser turn-on, a ~3.4 V level baseline from the nIR signal and the 3D sensor tip was stably observed for at least a few minutes without baseline drift or noise. Thereafter, the baseline remained stable even after continuous mechanical deformation of the optode fiber. We conclude that the tip design and adhesion are adequately integrated with the end of the optode fiber. Hence, the fully integrated lab-on-fiber system has potential for direct application to biopharmaceutical processing environments.

https://dx.doi.org/10.1021/acsnano.0c03417
ACS Nano 2020, 14, 10141−10152

We investigated whether the platform could be extended to the monitoring of other small-molecule analytes. For this, we created alternate 3D sensor tips with glass window integration for liquid phase monitoring of various solution phase bioanalytes (Figure 5). For the IgG aggregation monitoring, nanosensors were imbedded in the hydrogel, which can maintain their own shape; thus the excitation laser could touch the bottom of the sensor layer through the hole of the sensor tip without any slide window integration. To maximize versatility, the design should allow testing of small liquid volumes but result in stable nIR signals, even from media in the form of whole droplets. To realize this, an 8 mm cover glass slide was compactly integrated between the nanosensor holder and the optode fiber adaptor using an O-ring (5 mm inside diameter, 8 mm outside diameter, 1.5 mm thick, Buna-N O-Ring, MSC #31958200), producing a monitoring window (left schematic of Figure 5a). After putting the glass window and O-ring in series on the printed screw adaptor, the nanosensor holder can be pushed and rotated to perfectly remove all leaking points in the 3D sensor tip (right CAD of Figure 5a). The photo and nIR images show the nanosensor phase within the glass window interfaced tip produced by the 3D-printed design (Figure 5b,c). The result is a lab-on-fiber system easily extended to biochemical analyte monitoring.

To test whether our fiber optic nanosensor is extendable to other analytes of interest, we tested serotonin (5-HT), norepinephrine (NE), adrenaline (±epinephrine; ±E), and hydrogen peroxide (H_2O_2), monitoring the dynamic response of each upon addition. For this, we used nanosensors modified as described previously using corona phase molecular recognition (CoPhMoRe) to create selective interfaces for target bioanalytes.[42,43] Specifically, DNA sequences including $(GT)_{15}$ GAT CTA AGG CGT GTAT (*e.g.*, C1), ss$(ATT)_{10}$, ATCAAGGCTCGAATTGTCCCTGAAATCT (*e.g.*, C2), and d$(GT)_{15}$ were utilized for selective monitoring of 5-HT, NE, ±E, and H_2O_2, respectively. These nanosensors produce turn-on fluorescent responses for NE and E and turn-off responses for 5-HT and H_2O_2.[44,45] Real-time fluorescence measurements with the optode fiber show distinct turn-on or turn-off responses as applicable analytes within short times (2 min) with a significantly high signal-to-noise ratio (∼126.66 (5-HT)) (Figure 5d−g). Distinct response behavior of each bioanalyte was attributed to specific DNA sequences, and (n, m) SWNT chiralities of each nanosensor formed unique molecular interfaces, leading to distinct location of the highest occupied molecular orbital (HOMO) and lowest unoccupied molecular orbital (LUMO).[42,46] The maximum sensor responses of each analyte for 2 min after exposure are presented in Figure 5h. The platform is clearly capable of rapid analysis of these distinct bioanalytes with small analyte volume additions (5 μL at 1 mM) and short response times.

For monitoring these various bioanalytes, 3D sensing tips were constructed for liquid phase nanosensor queries without hydrogel immobilization. To measure the effect of the hydrogel tunable layer on small-molecule diffusion, 5-HT responses were compared with and without the hydrogel system (Figure 5i). The SWNT/ss$(GT)_{15}$ nanosensor for 5-HT was immobilized in the identical conditions of the IgG-monitoring 3D sensing tip with a hydrogel (0.2% agarose, expected hydrogel thickness: 420 μm). In the absence of a hydrogel layer, 5-HT injection caused an immediate drop in the sensor signal and reached the 90% of saturation level within 3.1 min. However, the addition of the hydrogel layer causes a demonstrable time lag in the sensor response and a slowing of the response dynamics such that the sensor response levels out only after several minutes. We note that the time scale of the experiment in Figure 5i is on the order of the diffusive time scale for a small molecule calculated via eq 4, assuming a hydrogel thickness of approximately 420 μm (from Figure 4e) and diffusion coefficient in agarose gel of 10^{-5} cm^2/s.[47]

$$\tau_D = \frac{L^2}{D} \approx \frac{(420\ \mu\text{m})^2}{1 \times 10^{-5}\ \text{cm}^2/s} = 176.4\ \text{s} \quad (4)$$

Hence, the hydrogel thickness needs to be considered when considering the detection time required for process monitoring. Overall, our optode fiber system could be universally applied to continuous and batch process monitoring of various biochemical analytes with versatile 3D sensing tip design and a wide range of nanosensor libraries.

CONCLUSIONS

In this work, we develop a fiber optic, benchtop instrument (optode) for the interrogation of fluorescent nanosensors both online and at-line for process monitoring and in manufacturing settings. We design and fabricate a compact, integrated fiber optic nanosensor element and characterize the sensitivity, response time, and stability for applications to rapid process monitoring. The optode fiber consists of label-free nIR fluorescent SWNT transducers embedded within a protective yet porous hydrogel attached to the end of the fiber waveguide. The optode is capable of differentiating the aggregation status of human IgG, reporting the relative fraction of monomers and dimer aggregates of IgG with sizes of 5.6 and 9.6 nm, respectively, in under 5 min of analysis time. A lab-on-fiber design shows potential for at-line protein monitoring with the integration of 3D-printed miniaturized sensor tips with mechanical flexibility. We also test the detection of other classes of bioanalytes (neurotransmitters, cytokines, ROS) using similar sensor constructs and were able to achieve high SNR at concentrations of interest, demonstrating that our fiber optic nanosensor system could be applied to various biochemical process monitoring. We envision this fiber optic system to be a vital component of coupling fluorescent based nanosensors into both continuous and batch process monitoring.

METHODS

Preparation and Characterization of SWNT Dispersions. All materials were purchased from Sigma-Aldrich unless stated otherwise. Highly purified CoMoCAT (6, 5)-enriched SWNTs were used for all experiments and were provided to us by Chasm Advanced Materials. Tissue culture-treated well plates (cat#: 25-104) were purchased from Genesee Scientific. Molecular biology agarose was purchased from Bio-Rad, and recombinant Protein A (rPA, His-tagged at N-terminus) was purchased from Abcam. Purified CoMoCAT SWNTs (1 mg) were mixed with 15 mL of 0.25 w% chitosan solution in 1 vol % acetic acid. This solution was tip sonicated (Qsonica Q125) using a 0.25 in. probe for 40 min in an ice bath at 10 W. The crude SWNT dispersion was centrifuged twice at 16000*g* for 90 min, in which the top 80% of the supernatant was collected each time. The concentration of the purified SWNT dispersion was approximated by collecting the absorption spectrum (Cary 5000, Agilent Technologies).

Nanosensor Synthesis. An agarose solution (0.2%) was prepared in distilled water and boiled until the agarose was completely melted. Once the solution cooled to about 60 °C, 50 μL aliquots were deposited on the bottom of a 96-well plate (25-104, Geness Scientific) and allowed to cure in a humidified environment at

https://dx.doi.org/10.1021/acsnano.0c03417
ACS Nano 2020, 14, 10141−10152

room temperature for 45 min. Approximately 15 μL of a 1 mg/L chitosan-SWNT solution was added atop each gel, and the well plate was placed in a humidified chamber at 38 °C for 60 min to promote diffusion of SWNTs into the hydrogel matrix. The well plate was later allowed to cool at room temperature for 15 min before washing each well with 150 μL of water to remove unbound SWNTs. Sensors were functionalized using a similar procedure to those reported previously.[30] First, a solution of 5 mg/mL succinic anhydride in 25× PBS was added atop the sensors to convert the primary amine groups to carboxylic acids. This reaction was allowed to proceed overnight. After washing the sensor gels two times with 150 μL of water, the carboxylic acid groups were activated by a solution of 20 mg/mL 1-ethyl-3-(3-(dimethylamino)propyl) carbodiimide (EDC) and 60 mg/mL *N*-hydroxy succinimide (NHS) in MES buffer for 2 h. Following this activation step, the sensors were washed two times with 150 μL of water and reacted with a solution of approximately 14 mM Cu(II) chelated by Cu-NTA. To create the Cu-NTA solution, 37 mg of NTA was combined with 170.5 mg of $CuCl_2 \cdot 2H_2O$ and 10 mL of 0.5× PBS. To precipitate out the excess, unchelated Cu(II) ions, the solution pH was raised to 7.5 via the addition of approximately 600 μL of 3 M NaOH. This solution was centrifuged at 1200 rpm for 7 min, after which the supernatant was used for reaction with the EDC/NHS-activated sensors.

Preparation of Analytes. Human agonist monoclonal (IgG_1) antibody (conatumumab, AMG 655) samples were provided to us by Amgen.[48] IgG_1 samples were provided in a formulation buffer containing 10 mM sodium acetate and 9% sucrose, at a pH of 5.2. Stressed IgG_1 samples were prepared by exposing 100 mg/mL solutions of IgG_1 to UV light for varying periods including 3, 7, and 74 h. UV exposure was performed in a stability chamber equipped with a UV lamp (wavelength range 320−400 nm) operating at a power of 22 W/m^2 at ambient temperature. Ten millimolar serotonin (5-hydroxytryptamin), adrenaline (±epinephrine), and (±)-norepinephrine (+)-bitartrate salt (Sigma-Aldrich) solutions were prepared with dimethyl sulfoxide (DMSO). Hydrogen peroxide (H_2O_2, 100 mM, Sigma-Aldrich) was prepared with a 0.1 M NaCl solution.

Optode Fiber Measurements. Sensors were excited with 561 nm (MGL-FN-561 200 mW, Opto Engine LLC/197 (length) × 70 (width) × 50 (height) mm^3, 2.0 kg) or 785 nm (MDL-III-785 500 mW, Opto Engine LLC) wavelengths. Here, versatile excitation sources including high-power LED could be coupled to the fiber optic platform for the benchtop mobile cart integration. The laser light propagates through fiber optic reflection/backscatter probe bundles (core diameter 200 μm, fiber length 2 m, weight 0.16 kg, RP29 Thorlabs) to the samples, and the fluorescence light propagates through the fiber to an InGaAs-amplified photodetector (PDF10C, Thorlabs). The fiber optic probe consists of 6 fibers around 1 fiber configuration where the central fiber provides the light delivery to the SWNT sensor hydrogel. The surrounding 6 fibers collect the near-infrared fluorescence light from the SWNT sensor hydrogel. To reduce laser scattering and autofluorescence at the hydrogel, a 900 nm short-pass filter and a 900 nm long-pass filter were inserted at the laser and photodetector, respectively. A focusing lens with a focal length of 30 mm was placed to efficiently collect fluorescence signal at a 0.5-mm-diameter active area of the photodetector. To suppress baseline noise from environments such as ceiling lamps, a black hardboard enclosure was placed around the samples and optode fiber. All the components of the instrument were loaded on a mobile cart (15Y320, Grainger, size: depth 18 in., width 24 in., height 26−42 in.). For the real-time signal measurement of IgG, 40 μL of PBS and 20 μL of protein A were added in series, and fluorescence signals were measured for 30 min. Then, 100 μL of PBS was injected twice to flush the remaining chemical and 10 μL of IgG solution was added to measure the signals. Usually, the signal saturated at 300−600 s. For the measurement of various bioanalytes, 50 μL of nanosensors was added in the sensor tip, and the baseline was measured for 5 min. Then, 5 μL of each analyte solution was added and signals were measured for 20 min. The 3D sensing tips were fabricated using a 3D-printer (Objet 30 Prime, Stratasys Ltd.) located in the Amgen Cambridge facility. The print was executed using "high quality" settings and VeroClear (PN: OBJ-04055, Stratasys) material with a minimum layer thickness of 16 μm. The prints were washed from the support material using an electric power washer (supplied by Stratasys). The resolution of 3D printer was *x*-axis: 600 dpi; *y*-axis: 600 dpi; *z*-axis: 1600 dpi; and the accuracy is 0.1 mm (0.0039 in.).

ASSOCIATED CONTENT

Supporting Information

The Supporting Information is available free of charge at https://pubs.acs.org/doi/10.1021/acsnano.0c03417.

Detailed explanation of multiple excitation laser sources of the optode fiber platform, detailed fabrication procedure for the custom-built optode fiber, continuous monitoring of laser power fluctuation using a power meter, optimized procedure for opto interfaces, fluorescence response of CHASM, HiPCO, and non-SWNT sensors, limit of detection for IgG monitoring, control experiment of IgG detection, detailed derivation of the hydrogel diffusion model, maximum measurement counts of a single 3D sensing tip (PDF)

AUTHOR INFORMATION

Corresponding Author

Michael S. Strano − *Department of Chemical Engineering, Massachusetts Institute of Technology, Cambridge, Massachusetts 02139, United States;* orcid.org/0000-0003-2944-808X; Email: strano@mit.edu

Authors

Daichi Kozawa − *Department of Chemical Engineering, Massachusetts Institute of Technology, Cambridge, Massachusetts 02139, United States;* orcid.org/0000-0002-0629-5589

Soo-Yeon Cho − *Department of Chemical Engineering, Massachusetts Institute of Technology, Cambridge, Massachusetts 02139, United States;* orcid.org/0000-0001-6294-1154

Xun Gong − *Department of Chemical Engineering, Massachusetts Institute of Technology, Cambridge, Massachusetts 02139, United States;* orcid.org/0000-0003-4168-2768

Freddy T. Nguyen − *Department of Chemical Engineering, Massachusetts Institute of Technology, Cambridge, Massachusetts 02139, United States;* orcid.org/0000-0003-0106-8114

Xiaojia Jin − *Department of Chemical Engineering, Massachusetts Institute of Technology, Cambridge, Massachusetts 02139, United States;* orcid.org/0000-0002-0694-5799

Michael A. Lee − *Department of Chemical Engineering, Massachusetts Institute of Technology, Cambridge, Massachusetts 02139, United States*

Heejin Lee − *Process Development, Amgen Inc., Cambridge, Massachusetts 02142, United States*

Alicia Zeng − *Process Development, Amgen Inc., Cambridge, Massachusetts 02142, United States*

Gang Xue − *Process Development, Amgen Inc., Cambridge, Massachusetts 02142, United States*

Jeff Schacherl − *Process Development, Amgen Inc., Cambridge, Massachusetts 02142, United States*

Scott Gibson − *Process Development, Amgen Inc., Cambridge, Massachusetts 02142, United States*

Leonela Vega − *Process Development, Amgen Inc., Cambridge, Massachusetts 02142, United States*

Complete contact information is available at:
https://pubs.acs.org/10.1021/acsnano.0c03417

Author Contributions

[§]D. Kozawa and S.-Y. Cho contributed equally to this work.

Notes

The authors declare no competing financial interest.

ACKNOWLEDGMENTS

The authors are grateful for a grant and SE-UPLC data from Amgen Inc. We acknowledge E. Poon, D. Salem, and L. Galindo (George R. Harrison Spectroscopy Laboratory) for constructive comments and guidance on the custom-built fiber construction. We thank T. T. S. Lew at Massachusetts Institute of Technology and G. Singh at the Disruptive & Sustainable Technology for Agricultural Precision (DiSTAP) Research Center in Singapore-MIT Alliance for Research and Technology Centre for helpful discussions. The authors are also grateful for support from the Walmart Foundation and the Walmart Food Safety Collaboration Center in Beijing. F.T.N. acknowledges the support of the Arnold O. Beckman Postdoctoral Fellowship.

REFERENCES

(1) Rantanen, J.; Khinast, J. The Future of Pharmaceutical Manufacturing Sciences. *J. Pharm. Sci.* **2015**, *104*, 3612−3638.

(2) Martin, N.; Ma, D.; Herbet, A.; Boquet, D.; Winnik, F. M.; Tribet, C. Prevention of Thermally Induced Aggregation of IgG Antibodies by Noncovalent Interaction with Poly(acrylate) Derivatives. *Biomacromolecules* **2014**, *15*, 2952−2962.

(3) Kastelic, M.; Kalyuzhnyi, Y. V.; Hribar-Lee, B.; Dill, K. A.; Vlachy, V. Protein Aggregation in Salt Solutions. *Proc. Natl. Acad. Sci. U. S. A.* **2015**, *112*, 6766−6770.

(4) Amin, S.; Barnett, G. V.; Pathak, J. A.; Roberts, C. J.; Sarangapani, P. S. Protein Aggregation, Particle Formation, Characterization & Rheology. *Curr. Opin. Colloid Interface Sci.* **2014**, *19*, 438−449.

(5) Schmit, J. D.; He, F.; Mishra, S.; Ketchem, R. R.; Woods, C. E.; Kerwin, B. A. Entanglement Model of Antibody Viscosity. *J. Phys. Chem. B* **2014**, *118*, 5044−5049.

(6) Pathak, J. A.; Sologuren, R. R.; Narwal, R. Do Clustering Monoclonal Antibody Solutions Really Have a Concentration Dependence of Viscosity? *Biophys. J.* **2013**, *104*, 913−923.

(7) Roberts, C. J. Protein Aggregation and Its Impact on Product Quality. *Curr. Opin. Biotechnol.* **2014**, *30*, 211−217.

(8) Jiskoot, W.; Randolph, T. W.; Volkin, D. B.; Middaugh, C. R.; Schöneich, C.; Winter, G.; Friess, W.; Crommelin, D. J. A.; Carpenter, J. F. Protein Instability and Immunogenicity: Roadblocks to Clinical Application of Injectable Protein Delivery Systems for Sustained Release. *J. Pharm. Sci.* **2012**, *101*, 946−954.

(9) Macdougall, I. C. Antibody-Mediated Pure Red Cell Aplasia (PRCA): Epidemiology, Immunogenicity and Risks. *Nephrol., Dial., Transplant.* **2005**, *20*, No. iv9-iv15.

(10) Berkowitz, S. A.; Engen, J. R.; Mazzeo, J. R.; Jones, G. B. Analytical Tools for Characterizing Biopharmaceuticals and The Implications for Biosimilars. *Nat. Rev. Drug Discovery* **2012**, *11*, 527−540.

(11) Kruss, S.; Hilmer, A. J.; Zhang, J.; Reuel, N. F.; Mu, B.; Strano, M. S. Carbon Nanotubes as Optical Biomedical Sensors. *Adv. Drug Delivery Rev.* **2013**, *65*, 1933−1950.

(12) Liu, Y.; Dong, X.; Chen, P. Biological and Chemical Sensors Based on Graphene Materials. *Chem. Soc. Rev.* **2012**, *41*, 2283−2307.

(13) Doria, G.; Conde, J.; Veigas, B.; Giestas, L.; Almeida, C.; Assuncao, M.; Rosa, J.; Baptista, P. V. Noble Metal Nanoparticles for Biosensing Applications. *Sensors* **2012**, *12*, 1657−1687.

(14) Holzmeister, P.; Acuna, G. P.; Grohmann, D.; Tinnefeld, P. Breaking the Concentration Limit of Optical Single-Molecule Detection. *Chem. Soc. Rev.* **2014**, *43*, 1014−1028.

(15) Ray, A.; Bristow, T.; Whitmore, C.; Mosely, J. On-Line Reaction Monitoring by Mass Spectrometry, Modern Approaches for the Analysis of Chemical Reactions. *Mass Spectrom. Rev.* **2018**, *37*, 565−579.

(16) Fekete, S.; Beck, A.; Veuthey, J. L.; Guillarme, D. Theory and Practice of Size Exclusion Chromatography for the Analysis of Protein Aggregates. *J. Pharm. Biomed. Anal.* **2014**, *101*, 161−173.

(17) Yu, Z.; Reid, J. C.; Yang, Y.-P. Utilizing Dynamic Light Scattering as a Process Analytical Technology for Protein Folding and Aggregation Monitoring in Vaccine Manufacturing. *J. Pharm. Sci.* **2013**, *102*, 4284−4290.

(18) Righetti, P. G.; Verzola, B. Folding/Unfolding/Refolding of Proteins: Present Methodologies in Comparison with Capillary Zone Electrophoresis. *Electrophoresis* **2001**, *22*, 2359−2374.

(19) Gong, X.; Park, M.; Parviz, D.; Silmore, K. S.; Gordiichuk, P.; Lew, T. T. S.; Strano, M. S. Single-Particle Tracking for Understanding Polydisperse Nanoparticle Dispersions. *Small* **2019**, *15*, 1901468.

(20) Silmore, K. S.; Gong, X.; Strano, M. S.; Swan, J. W. High-Resolution Nanoparticle Sizing with Maximum A Posteriori Nanoparticle Tracking Analysis. *ACS Nano* **2019**, *13*, 3940−3952.

(21) Wang, W. Protein Aggregation and Its Inhibition in Biopharmaceutics. *Int. J. Pharm.* **2005**, *289*, 1−30.

(22) Zölls, S.; Tantipolphan, R.; Wiggenhorn, M.; Winter, G.; Jiskoot, W.; Friess, W.; Hawe, A. Particles in Therapeutic Protein Formulations, Part 1: Overview of Analytical Methods. *J. Pharm. Sci.* **2012**, *101*, 914−935.

(23) Hong, M. S.; Severson, K. A.; Mo, J.; Lu, A. E.; Love, J. C.; Braatz, R. D. Challenges and Opportunities in Biopharmaceutical Manufacturing Control. *Comput. Chem. Eng.* **2018**, *110*, 106−114.

(24) Ündey, C.; Ertunç, S.; Mistretta, T.; Looze, B. Applied Advanced Process Analytics in Biopharmaceutical Manufacturing: Challenges and Prospects in Real-Time Monitoring and Control. *J. Process Control* **2010**, *20*, 1009−1018.

(25) Reuel, N. F.; Grassbaugh, B.; Kruss, S.; Mundy, J. Z.; Opel, C.; Ogunniyi, A. O.; Egodage, K.; Wahl, R.; Helk, B.; Zhang, J. Q.; Kalcioglu, Z. I.; Tvrdy, K.; Bellisario, D. O.; Mu, B.; Blake, S. S.; Van Vliet, K. J.; Love, J. C.; Wittrup, K. D.; Strano, M. S. Emergent Properties of Nanosensor Arrays: Applications for Monitoring IgG Affinity Distributions, Weakly Affined Hypermannosylation, and Colony Selection for Biomanufacturing. *ACS Nano* **2013**, *7*, 7472−7482.

(26) Zhang, J. Q.; Kruss, S.; Hilmer, A. J.; Shimizu, S.; Schmois, Z.; De La Cruz, F.; Barone, P. W.; Reuel, N. F.; Heller, D. A.; Strano, M. S. A Rapid, Direct, Quantitative, and Label-Free Detector of Cardiac Biomarker Troponin T Using Near-Infrared Fluorescent Single-Walled Carbon Nanotube Sensors. *Adv. Healthcare Mater.* **2014**, *3*, 412−423.

(27) Nelson, J. T.; Kim, S.; Reuel, N. F.; Salem, D. P.; Bisker, G.; Landry, M. P.; Kruss, S.; Barone, P. W.; Kwak, S.; Strano, M. S. Mechanism of Immobilized Protein A Binding to Immunoglobulin G on Nanosensor Array Surfaces. *Anal. Chem.* **2015**, *87*, 8186−8193.

(28) Dong, J. Y.; Salem, D. P.; Sun, J. H.; Strano, M. S. Analysis of Multiplexed Nanosensor Arrays Based on Near-Infrared Fluorescent Single-Walled Carbon Nanotubes. *ACS Nano* **2018**, *12*, 3769−3779.

(29) Paschotta, R. Noise in Laser Technology. *Opt. Photonik* **2009**, *4*, 48−50.

(30) Salem, D. P.; Gong, X.; Lee, H.; Zeng, A.; Xue, G.; Schacherl, J.; Gibson, S.; Strano, M. S. Characterization of Protein Aggregation Using Hydrogel-Encapsulated nIR Fluorescent Nanoparticle Sensors. *ACS Sens.* **2020**, *5*, 327−337.

(31) Shah, D. D.; Zhang, J. M.; Maity, H.; Mallela, K. M. G. Effect of Photo-Degradation on the Structure, Stability, Aggregation, and

Function of an IgG_1 Monoclonal Antibody. *Int. J. Pharm.* **2018**, *547*, 438−449.
(32) Lorenz, C. M.; Wolk, B. M.; Quan, C. P.; Alcala, E. W.; Eng, M.; McDonald, D. J.; Matthews, T. C. The Effect of Low Intensity Ultraviole C Light on Monoclonal Antibodies. *Biotechnol. Prog.* **2009**, *25*, 476−482.
(33) Pan, H.; Chen, K.; Chu, L.; Kinderman, F.; Apostol, I.; Huang, G. Methionine Oxidation in Human IgG_2 Fc Decreases Binding Affinities to Protein A and FcRn. *Protein Sci.* **2009**, *18*, 424−433.
(34) Bertolotti-Ciarlet, A.; Wang, W. R.; Lownes, R.; Pristatsky, P.; Fang, Y. L.; McKelvey, T.; Li, Y.; Li, Y.; Drummond, J.; Prueksaritanont, T.; Vlasak, J. Impact of Methionine Oxidation on The Binding of Human IgG_1 to FcRn and Fc Gamma Receptors. *Mol. Immunol.* **2009**, *46*, 1878−1882.
(35) Liang, S. M.; Xu, J.; Weng, L. H.; Dai, H. J.; Zhang, X. L.; Zhang, L. N. Protein Diffusion in Agarose Hydrogel *In Situ* Measured by Improved Refractive Index Method. *J. Controlled Release* **2006**, *115*, 189−196.
(36) Crank, J. *The Mathematics of Diffusion*, 2nd ed.; Clarendon Press: Oxford, 1979.
(37) Amsden, B. Solute Diffusion within Hydrogels. Mechanisms and Models. *Macromolecules* **1998**, *31*, 8382−8395.
(38) Pluen, A.; Netti, P. A.; Jain, R. K.; Berk, D. A. Diffusion of Macromolecules in Agarose Gels: Comparison of Linear and Globular Configurations. *Biophys. J.* **1999**, *77*, 542−552.
(39) Ricciardi, A.; Crescitelli, A.; Vaiano, P.; Quero, G.; Consales, M.; Pisco, M.; Esposito, E.; Cusano, A. Lab-On-Fiber Technology: A New Vision for Chemical and Biological Sensing. *Analyst* **2015**, *140*, 8068−8079.
(40) Kostovski, G.; Stoddar, P. R.; Mitchell, A. The Optical Fiber Tip: An Inherently Light-Coupled Microscopic Platform for Micro- and Nanotechnologies. *Adv. Mater.* **2014**, *26*, 3798−3820.
(41) Elsherif, M.; Moreddu, R.; Hassan, M. U.; Yetisen, A. K.; Butt, H. Real-Time Optical Fiber Sensors Based on Light Diffusing Microlens Arrays. *Lab Chip* **2019**, *19*, 2060−2070.
(42) Zhang, J. Q.; Landry, M. P.; Barone, P. W.; Kim, J. H.; Lin, S. C.; Ulissi, Z. W.; Lin, D. H.; Mu, B.; Boghossian, A. A.; Hilmer, A. J.; Rwei, A.; Hinckley, A. C.; Kruss, S.; Shandell, M. A.; Nair, N.; Blake, S.; Sen, F.; Sen, S.; Croy, R. G.; Li, D. Y.; et al. Molecular Recognition Using Corona Phase Complexes Made of Synthetic Polymers Adsorbed on Carbon Nanotubes. *Nat. Nanotechnol.* **2013**, *8*, 959−968.
(43) Bisker, G.; Dong, J.; Park, H. D.; Iverson, N. M.; Ahn, J.; Nelson, J. T.; Landry, M. P.; Kruss, S.; Strano, M. S. Protein-Targeted Corona Phase Molecular Recognition. *Nat. Commun.* **2016**, *7*, 10241.
(44) Zhang, J.; Boghossian, A. A.; Barone, P. W.; Rwei, A.; Kim, J.-H.; Lin, D.; Heller, D. A.; Hilmer, A. J.; Nair, N.; Reuel, N. F.; Strano, M. S. Single Molecule Detection of Nitric Oxide Enabled by $d(AT)_{15}$ DNA Adsorbed to Near Infrared Fluorescent Single-Walled Carbon Nanotubes. *J. Am. Chem. Soc.* **2011**, *133*, 567−581.
(45) Jeong, S.; Yang, D.; Beyene, A. G.; Bonis-O'Donnell, J. T. D.; Gest, A. M. M.; Navarro, N.; Sun, X.; Landry, M. P. High-Throughput Evolution of Near-Infrared Serotonin Nanosensors. *Sci. Adv.* **2019**, *5*, No. eaay3771.
(46) Salem, D. P.; Landry, M. P.; Bisker, G.; Ahn, J.; Kruss, S.; Strano, M. S. Chirality Dependent Corona Phase Molecular Recognition of DNA-Wrapped Carbon Nanotubes. *Carbon* **2016**, *97*, 147−153.
(47) Lundberg, P.; Kuchel, P. W. Diffusion of Solutes in Agarose and Alginate Gels: 1H and 23Na PFGSE and 23Na TQF NMR Studies. *Magn. Reson. Med.* **1997**, *37*, 44−52.
(48) Bajaj, M.; Heath, E. I. Conatumumab: A Novel Monoclonal Antibody against Death Receptor 5 for the Treatment of Advanced Malignancies in Adults. *Expert Opin. Biol. Ther.* **2011**, *11*, 1519−1524.

https://dx.doi.org/10.1021/acsnano.0c03417
ACS Nano 2020, 14, 10141−10152